Journal of Solid State Chemistry 308 (2022) 122890

Contents lists available at ScienceDirect

Journal of Solid State Chemistry

journal homepage: www.elsevier.com/locate/jssc

Aliphatic mixed ligands Sn(II) complexes as photon absorbers in quantum dots sensitized solar cell

Mojeed A. Agoro [a,b], Edson L. Meyer [b], Johannes Z. Mbese [a], Xolile Fuku [c], Chinedu C. Ahia [b,*]

[a] Department of Chemistry, University of Fort Hare, Private Bag X1314, Alice, 5700, South Africa
[b] Fort Hare Institute of Technology, University of Fort Hare, Private Bag X1314, Alice, 5700, South Africa
[c] Institute of Nanotechnology and Water Sustainability (iNanoWS), College of Science, Engineering and Technology, Florida campus, UNISA, South Africa

ARTICLE INFO

Keywords:
Dye solar cell
Quantum dots
Tin sulfide
Thermal-decomposition
Electrochemical
Molecular precursor

ABSTRACT

Dye-sensitized solar cells have attracted a lot of research interest due to the quest for an alternative energy supply given that it is cost-effective and its materials are easily available. However, the need to improve the conversion efficiency of these solar cell devices has necessitated the search for new materials that will lead to more energy conversion. One of such material of interest is tin (II) sulfide (SnS). In present study, we report results from the synthesis of hexadecylamine (HDA)-capped SnS and uncapped SnS photosensitizer using a molecular precursor. The efficiency of the photon absorbers, their morphological, structural and electrochemical properties were examined using different techniques. Both photosensitizers displayed X-ray diffraction (XRD) peaks within the range 26.03°–66.05°, which corresponds to orthorhombic structure. Field Emission Scanning Electron Microscope (FE-SEM) and High-Resolution Transmission Electron Microscope (HRTEM) further revealed that HDA-capped SnS has a better morphology and size distribution. UV–Vis analysis shows that the HDA-capped SnS exhibits strong absorption in the entire visible region which is attributed to perfect orientation. The HDA-capped photosensitizer superiority was linked to well reduced electron recombination and electron lifetime. The addition of HDA capping agent improved the *J-V* performance with a new conversion efficiency of 8.20%. Results obtained from present work proselytize the concept of using capping agent as an approach for improving the quality of photon absorbers.

1. Introduction

Providing an affordable and sustainable source of energy to meet the ever-growing energy demand has prompted researchers to focus on solar photovoltaic (PV) source of energy that will enhance and sustain the world economic growth. Solar photovoltaic has promising prospects based on the conversion efficiency obtained from materials like cadmium telluride (CdTe), wafers, copper indium gallium selenide (CIGS) and crystalline silicon (c-Si) [1]. One major challenge of PV electricity remains the price of electricity per kWh. This limitation can be solved by reducing the production cost or enhancing the conversion efficiency, with new materials that are less toxic and better conversion efficiency. Developing cost-friendly and environmentally hazard-free materials in abundance, benefits not only the PV market but also the ecosystem [1–3]. The increasing interest in thin-film semiconductors is linked to their potentials in solid-state applications, like photoelectrochemical, photovoltaic, solar cells, photoconductive cells, sensors, polarizers and many more [4,5]. SnS has distinguished itself among metal chalcogenides with excellent characteristics such as environmental friendliness, cheapness, non-toxicity and natural abundance [6,7]. SnS is employed in various applications such as lithium-ion batteries, gas sensors, photocatalysts, electrical switching, optoelectronic and solar cells due to its suitable properties. Furthermore, the high absorption coefficient of 10^4 cm^{-1} at wavelength range 400–1200 nm makes SnS more suitable for photovoltaic applications such as quantum dot sensitized solar cells (QDSSCs) which deals with the shortfall of ideal dyes sensitized solar cell DSSCs [7–13]. This accounts for the adoption of SnS as an absorber layer in photovoltaic applications.

However, the highest recorded conversion efficiency of SnS is 4.4% which is a major shortfall in the thin-film solar cells [14]. This limitation is directly linked to the grain size of SnS resulting in defects of the high-density grain boundary, which acts as carrier recombination centres [14–16]. This carrier recombination affects conversion efficiency and low open-circuit voltage (*Voc*), which is due to off-stoichiometry, poor

* Corresponding author.
E-mail address: chinedu@aims.ac.za (C.C. Ahia).

https://doi.org/10.1016/j.jssc.2022.122890
Received 12 November 2021; Received in revised form 27 December 2021; Accepted 7 January 2022
Available online 10 January 2022

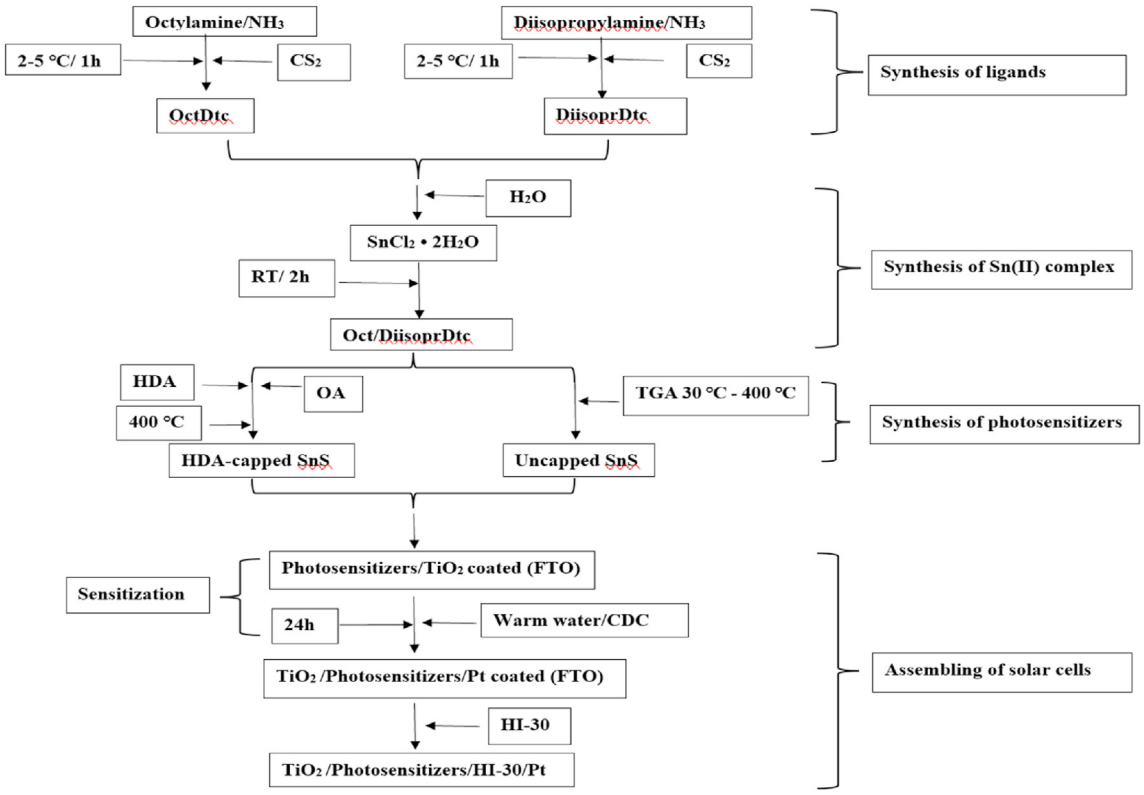

Scheme. 1. Schematic diagram for the fabrication and assembling of uncapped SnS and HDA-capped SnS photosensitizer in QDSSCs.

morphology, impurity arising from defects inside the thin-film and misaligned bandgap near the interface [15,17]. Other challenges such as uneven morphology or thickness, misfits of the electrical contacts between the buffer and SnS layer resulted in many defects inside the film [15,18,19]. Also, higher temperature on the substrate surface may cause multiple nucleation centres, increased density of defects and mid band gap trap levels [2]. Therefore, the introduction of a new and better material that will enhance the microstructure and surface morphology through different deposition approaches and post-treatment condition is vital [8]. Various approaches have been adopted for the fabrication of SnS thin films such as hydrothermal, electrochemistry, pulse electrodeposition, sulfurization, radio frequency (RF) sputtering, chemical vapour deposition, atomic layer deposition, successive ionic layer adsorption and reaction (SILAR), vacuum evaporation, chemical bath deposition, direct deposition and chemical spray pyrolysis [6,20–23]. However, these approaches could not give precise size distribution. The single-source precursor approach has produced high quality quantum dots (QDs) nanocrystals size and shape at low temperature, using capping agents as a catalyst to protect the surface morphology [24,25]. The present study employed the single-source molecular precursor route to synthesize SnS QDs photosensitizes, with better structural, morphological and particles size distribution. The direct deposition was used to sensitize the coated titanium dioxide (TiO_2) with SnS QDs photosensitizers by immersing both together for 24 h in a solution. This study reports on the characterization and performance of SnS-nanocrystal sensitizers thermalized from a molecular precursor.

2. Materials and methods

2.1. Materials

All solvents were of the highest purity (99.9%), supplied by Merck (Johannesburg, South Africa) and were used without further purification. Ammonia solution, diethyl ester, carbon disulphide (CS_2), methanol, toluene, octylamine, Iso-propane amine, tin (II)Chloride dihydrate ($SnCl_2 \bullet 2H_2O$) salts, water, oleic acid (OA), methanol and hexadecylamine (HDA). The complete test kits containing platinum and TiO_2 Fluorine-doped Tin Oxide (FTO) substrate, iodide HI-30 electrolyte, chenodeoxycholic acid (CDC), masks, hot seal and gaskets were supplied by Solaronix Company (Aubonne, Switzerland).

2.2. Synthesis of bis(N-diisopropyl-N-octyldithiocarbamato)tin(II) ligands and complexes

In a distinctive synthesis process as seen in (Scheme 1), a blend of octylamine of (16.5480 mL) and (30 mL) of ice-cold ammonia aqueous concentration was added with ice-cold CS_2 of (6.043 mL) and stirred for 1 h. A white precipitate colour was formed; this was later washed with diethyl ether and dried before characterization. Yield: ((14.8493g) (89.74%)). ^{1}H-NMR (400 MHz, DMSO-d_6, δ): = 2.50 (s, 6H, DMSO), 3.22–3.39, (6H, m, –CH_3). Selected IR (KBr): ν = 1470 (C–N), 939 (C–S), 3195 (N–H), 2920 (CH_3), 2955 (CH_2). Ammonium *N*-diisopropyldithiocarbamate (Di-IsoprDTC) ligands were prepared following a similar procedure, using (9.64 mL) (0.1 mol) of Di-IsoprDTC. Yield: ((1.462g) (32.00%)). ^{1}H-NMR (400 MHz, DMSO-d_6, δ): = 1.3 (t, 2H,–CH_2), 3.4 (s, 2H,–NH), 0.9 (t, 3H,–CH_3). Selected IR (KBr): ν = 1470 (C–N), 1095 (C–S), 3381 (N–H), 2821 (CH_3).

For the complexes, metal salts of tin (II) Chloride dehydrate ($SnCl_2 \bullet 2H_2O$) (0.6953g (2.5 mmol)) was mixed with distilled water of (15 mL) and added to (0.4859g (2.5 mmol)) of disoprDTC and OctDTC of (0.5555g (2.5 mmol)) was dissolved in (15 mL) of distilled water at ratio 1:1:1. The synthesis was stirred for 2h at room temperature (RT). As soon as the final products was obtained, the synthesis was completed by the filtration and washing of the products with methanol. The synthesized complex was dried at RT. Yield: (0.7707g (48.01%)), melting point: (202.7–204.9°C). ^{1}H-NMR (400 MHz, DMSO-d_6, δ): = 2.50 (s, 6H,

DMSO), 1.3 (s, 2H–CH_2), 0.9 (t, 3H–CH_3). Selected IR (KBr): $\nu = 1511$ (C–N), 1033 (C–S), 577 (M − S), 3210 (N–H), 2953 (CH_3), 2923 (CH_2).

2.3. Synthesis of uncapped and HDA-capped SnS nanoparticles

PerkinElmer TGA 4000 ThermoGravimetric Analyser (TGA) was utilized to synthesize the uncapped SnS nanocrystals through the thermal breakdown of *bis*(*N*-diisopropyl-*N*-octyl dithiocarbamato)tin (II) complexes [26,27]. The end-product of the complexes was obtained as residue, which resulted in the formation of uncapped SnS nanocrystals from the final mass residue. HDA-capped SnS was synthesized according to the literature method [28,29], while 3g of HDA was mixed with 0.20g of *bis*(*N*-diisopropyl-*N*-octyldithiocarbamato)tin (II) complexes and 4 mL of OA at 400 °C to control the particle size and for surface passivation. 20–30°C initial temperature was attained for the mixture of HDA to boil. The reaction was stabilized at 400 °C and the process lasted for 1 h. The reaction temperature was reduced to 70 °C afterwards 20 mL and about 50 mL of methanol were used to remove excess HDA and OA. Centrifugation was used to partition the flocculent precipitate at 3500 rpm and 2058g equivalent for 30 min, and then the supernate was poured off and washed several times. Low air pressure was used to remove the solvent giving rise to HDA-capped SnS nanoparticles.

2.4. Fabrication and assembling of QDSSCs

QDSSCs was assembled according to literature [30] using FTO glass substrate electrodes, 2×2 cm^2 of Platinum (Pt) and TiO_2 with 6×6 mm^2 active areas coated paste. Sensitization of the synthesized HDA-capped SnS and uncapped SnS was done using warm water of 10 mL for each samples with addition of co-adsorbents of CDC. TiO_2 electrode was immersed into the photosensitizers solution for 24 h. Commercial HI-30 iodide electrolyte at 0.05 M was utilized as mediating solution. The two FTO glass substrate electrodes were held together, one coated with Pt and the other with TiO_2 along with the photosensitizers using polyethylene and soldering iron. While the HI-30 iodide electrolyte was injected using syringe.

2.5. Physical measurements

To understand the optical behaviour of the as-synthesized photosensitizers, (1) thermal, (2) optical, (3) structural, (4) morphological and (5) electrical techniques were used. (1) PerkinElmer TGA 4000 ThermoGravimetric analyser. (2) Absorption spectra were obtained from UV–Vis spectrophotometer from PerkinElmer LAMBDA 365 and the Photoluminescence of the nanomaterials was evaluated by LS 45 fluorimeter from PerkinElmer. (3) NMR analysis was obtained from Bruker AV-400 spectrometer operating at 400.13 MHz, 300 K, and a spinning rate at 4 kHz. PerkinElmer Fourier Transform InfraRed (FTIR) spectrophotometer with attenuated total reflection (ATR) resolution mode at 4 cm^{-1} utilizing a KBr/Ge beam splitter, ceramic light source, and a lithium tantalate ($LiTaO_3$) detector scanning from 4000 to 370 cm^{-1} in order to identify the absorption spectrum of the functional groups of the materials. X-ray diffractometer was used to confirm the structural pattern of both photosensitizers at the interval of 0.05° between 10 and 90°. Raman spectra were obtain from a Confocal Raman AFM Imaging system (WiTec GmbH) alpha300RS. A fiber coupled laser of wavelength 532 nm that has an output power of 44 mW and a great yield control was utilize as the excitation source. (4) FE-SEM Zeiss Auriga SEM outfitted with Energy Dispersive X-Ray Spectroscopy were employed to identify the elemental composition and the morphology of the photosensitizers were investigated at 30 KV using JEOL JEM 2100 HRTEM operating at 200 kV. (5) Electrochemical evaluation were carried out using Metrohm 85695 Autolab, while Platinum and TiO_2 electrodes, with HI-30 iodide electrode were used as reference electrodes. Cyclic voltammetry was performed at scan rates between 0.05 and 0.35 V s^{-1} with an increment of 0.05 V s^{-1}. Electrochemical impedance spectroscopy (EIS) was carried out in the frequency range between 100 kHz and 100 mHz. Current density-voltage were collected through a Keithley 2401 source meter and a Thorax light power meter. Lumixo AM1.5 light simulator and the lamp was fixed at 50 cm and kept below 25°C at 100 mW cm^{-2} (AM1.5) to avoid cells degradation.

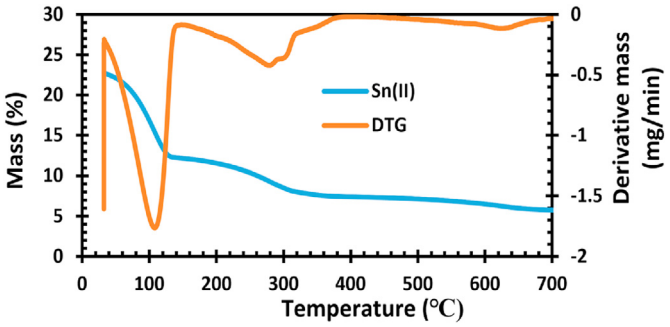

Fig. 1. TGA Spectra of *bis*(*N*-diisopropyl-*N*-octyldithiocarbamato)Sn(II).

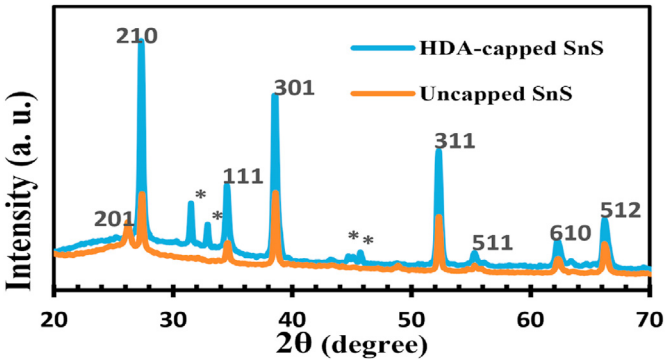

Fig. 2. XRD spectra of HDA-capped SnS and uncapped SnS nanoparticles.

3. Results and discussion

3.1. ThermoGravimetric analyser (TGA)

TGA and Derivative thermogravimetric (DTG) spectra of *bis*(*N*-diisopropyl-*N*-octyldithiocarbamato) Sn (II) precursor is presented in Fig. 1. From Fig. 1, the thermal decomposition formations of Sn involves two steps. The first breakdown step which occurred at 122 °C is due to the presence of a small amount of moisture in the sample. The second decomposition at 316 °C is linked to *N*-diisopropyl-*N*-octyldithiocarbamato ligand moiety, signifying the complete loss of organic moieties of the ligands. The remaining mass residue contains the end product (uncapped SnS) with 5.7% [31].

3.2. X-ray diffraction (XRD)

X-ray diffraction was employed to obtain the phase and structural properties of HDA-capped SnS and the uncapped SnS nanoparticles. The XRD patterns of HDA-capped SnS and uncapped SnS photosensitizers are shown in Fig. 2. Eleven peaks of 2θ angle from 27.02° to 66.05° for the HDA-capped SnS and 26.03°–66.04° for the uncapped SnS were measured respectively. The XRD plots corresponds to orthorhombic SnS structure (according to JCPDS 039–0354). The nanostructures were polycrystalline which were confirmed by the HRTEM micrographs shown in Fig. 5, with orientation along (201), (210), (111), (301), (311), (511), (610) and (512) for both photon absorbers.

The growth process through nucleation control revealed a preferential orientation of uncapped SnS and HDA-capped SnS [32,33]. It was very clear that the (210) peaks were more intense in HDA-capped SnS

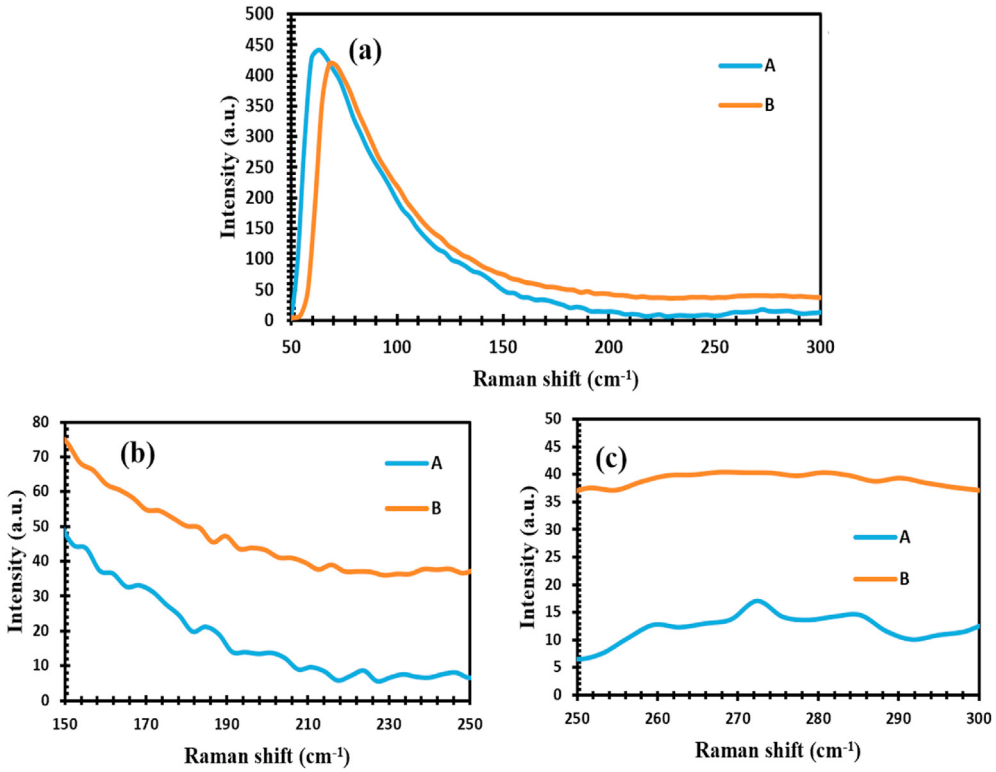

Fig. 3. Ramam spectra (a–c) A = HDA-capped SnS, B = uncapped SnS nanoparticles.

compared to uncapped SnS, indicating an improvement in crystallinity. Other peaks at 31.4°, 32.9°, 44.7° and 45.7° for HDA-capped SnS is due to impurity from the HDA capping agent. The quality of HDA-capped SnS could be linked to nucleating centres from the molecular precursor atoms which favour the growth of SnS [34]. The crystallite size (D) and full width at half maximum (FWHM) values of (111) peaks for the uncapped SnS are 27.96 nm and 0.2587°, and 30.27 nm and 0.2523° for the HDA-capped SnS. The size distributions increased for the capped SnS due to the addition of HDA, while the presence of crystal defects and lattice distortions in the uncapped SnS resulted in a decreased crystalline quality of the uncapped SnS.

Orthorhombic SnS structure with space group *Pnma-B16 2h* exhibits four unit cell molecules. This structure which is described as pseudo-tetragonal have 'Sn' atom each surrounded by six 'S' atoms, three at a shorter distance and three atoms at a longer distance. This is in agreement with XRD observations of the standard d-spacing values which corresponds to the (110) and (111) lattice planes of the orthorhombic SnS.

The Raman spectra for the uncapped and HDA-capped SnS is shown in Fig. 3(a–c). As previously described [35], orthorhombic structures has been reported with 24 vibrational modes;

$$\Gamma = 4A_g + 2B_{1g} + 4B_{2g} + 2B_{3g} + 2A_u + 4B_{1u} + 2B_{2u} + 4B_{3u}$$

while 21 optical phonons were observed, seven were infrared active ($3B_{1u}$, $3B_{3u}$, and $1B_{2u}$), two were inactive ($2A_u$), and 12 were Raman active ($4A_g$, $2B_{1g}$, $4B_{2g}$, and $2B_{3g}$). The Raman spectra shows identical patterns for both photosensitizers with slight peak intensity variations. Strong lattice vibrations which occurred at 66 and 71 cm^{-1} are ascribable to the B_{1g} modes as a result of the difference in concentrations of the active groups. The vibrations at 171-290 cm^{-1} are associated with the SnS primary phase [36] and identified in present study as A_g and B_{2g} Raman active modes. The appearance of a given mode depends on the incident and scattering radiation directions parallel to any of the three axis (a, b, c), scattered photons and electrical polarization of the incidence [37]. Specifically, the vibrations at 176, 219, 228 and 280 cm^{-1} for uncapped

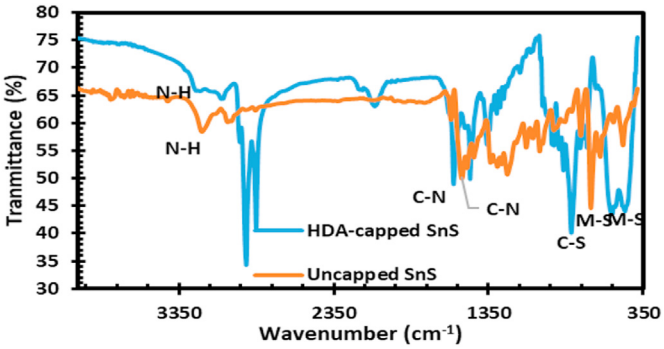

Fig. 4. FTIR spectra of HDA-capped SnS and uncapped SnS nanoparticles.

SnS and peaks at 171, 214, 227 and 272 cm^{-1} for HDA-capped SnS are associated with the A_g modes. These peaks positions corresponds with the α-phase SnS from literature. Furthermore, the Raman peaks at 189, 290 cm^{-1} for uncapped SnS and 188, 285 $cm^{-1}$for HDA-capped SnS respectively are ascribed to B_{2g} Raman modes [38,39].

From the photosensitizers reported in this study, the sharp and broad peaks of υ(M − S) band displayed at 555 cm^{-1} and 692 cm^{-1} for HDA-capped SnS and uncapped SnS are ascribed to the symmetrical moiety of the ligands as seen in Fig. 4. The IR spectra of HDA-capped SnS exhibits strong intensity, a characteristics which indicates the presence of single band, possibly due to υ(C–S) vibration at 816 cm^{-1}. The υ(C–N) peaks were found at 1577 $cm^{-1}$and 1524 cm^{-1} for HDA-capped SnS and the uncapped SnS respectively. This implies a substantial double bond attractiveness of the C–N bond with the complexes. The υ(N–H) vibrations of the coordinating amines were observed in the region between 3200 and 3297 cm^{-1}. The injection of capped agents reveals a change in the vibration shift for both photosensitizers and the presence of others. This trend is similar to the observation in the XRD result for the HDA capped SnS [40–42].

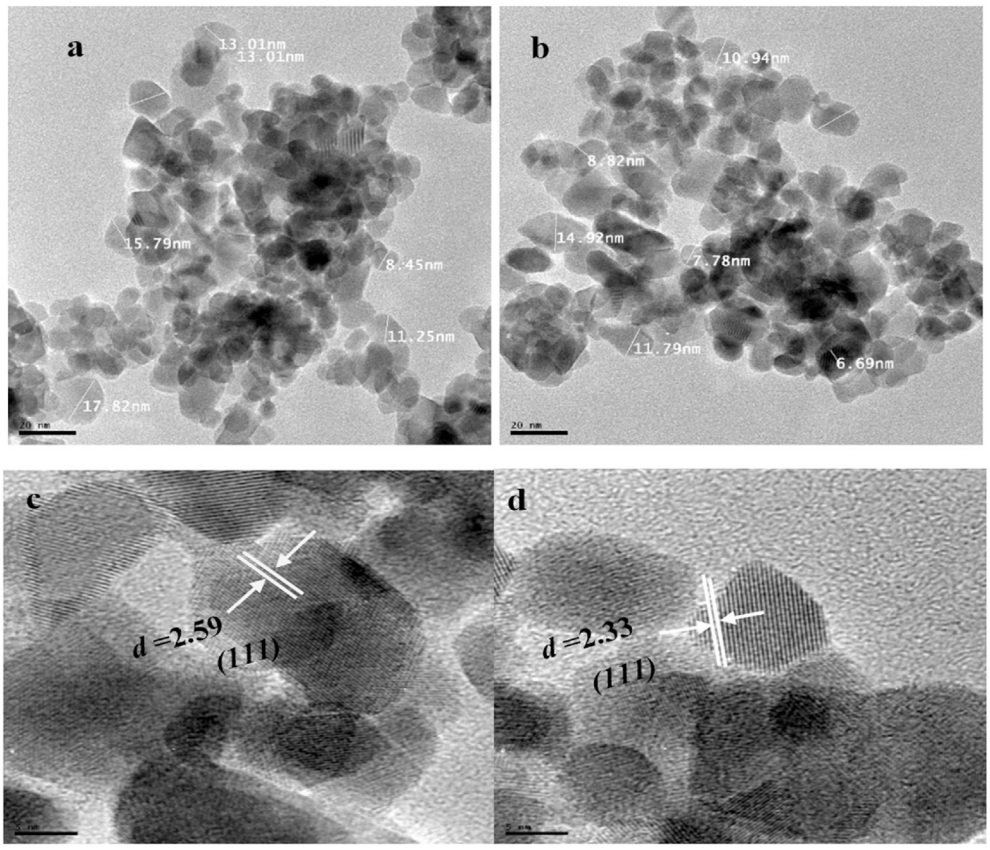

Fig. 5. HRTEM image of (a, c) for uncapped SnS and (b, d) HDA-capped SnS nanoparticles.

Table 1
Raman modes for uncapped and HDA-capped SnS photosensitizers.

Character and Symmetry and Experimental values		
Character and symmetry	Uncapped SnS (cm^{-1})	HDA-capped SnS (cm^{-1})
B_{1g}	71	66
A_g	176	171
B_{2g}	189	188
A_g	219	214
A_g	228	227
A_g	280	272
B_{2g}	290	285

The experimental values of some Raman active modes obtained from this study for both samples are summarized in Table 1.

3.3. HRTEM

The HRTEM images of HDA-capped SnS and uncapped SnS photosensitizer nanoparticles are shown in Fig. 5(a–d). The images reveal a co-existence of amorphous phases and orthorhombic phase with a size distribution of 8.45 nm–17.82 nm as seen in Fig. 5 (a) and (c) for the uncapped SnS, while the HDA-capped SnS which are shown in Fig. 5 (b) and (d) revealed particles sizes in the range of 6.69 nm–14.92 nm with orthorhombic crystalline [43,44], which can be indexed to the (111) planes of SnS. The HRTEM images further provides the lattice fringes with interplanar lattice spacing of 2.33 nm for HDA-capped SnS and 2.59 nm for the uncapped SnS which is indexed to the (110) planes of orthorhombic SnS nanoparticles. The co-existence of both the amorphous and crystalline orthorhombic phases for uncapped SnS photosensitizer reveals poor lattice fringes due to its amorphous nature, which could be linked to the high-temperature effect on molecular precursor during TGA decomposition. This factor influences the performances of photovoltaic cells, which can be confirmed through the *J-V* results obtained for HDA-capped SnS which exhibits better performance compared to uncapped SnS.

3.4. FE-SEM

FE-SEM images of HDA-capped SnS and uncapped SnS consist of agglomerated nanocrystals, micro-sized spherical particles with dense clusters as seen in Fig. 6(a–d). This indicates that the molecular precursor was beneficial as a vital tool in the uniform morphology and growth control of HDA-capped SnS and uncapped SnS. Besides, it is well known that alkyl group with long-chain gives rise to better crystalline and shaped particles, which have a great influence on the particle size, shape and morphology of HDA-capped SnS and uncapped SnS [45,46]. The results obtained in present study is similar to the morphology observed by Hortikar et al. [47]. In order to identified the effect of sensitization and their influence on the layer thickness coated on TiO_2, the SEM cross sectional images of uncapped SnS and HDA-capped SnS photosensitizers are provided in Fig. 6(e) and (f). The measured thicknesses for the layers coated with TiO_2 electrode are 750.6 nm and 860.3 nm. The comparison of the thicknesses values suggests an increased quantity of the HDA-capped SnS compared to the TiO_2 electrode which accounts for the increased thicknesses. These results justified the I–V efficiency enhancement of 0.37% for HDA-capped SnS compared to the uncapped SnS cell efficiency. The enhancement of coated TiO_2 thickness is associated with the increased absorption of light-harvesting which is explained by the Beer−Lambert law [48] since the film thickness is inversely proportional to the transmitted light intensity, which results in more light absorption by increasing the film thickness. This further cemented the CV results indicating that the highest number of electrons are produced due to photon absorption by this photosensitizers coated on the TiO_2 electrode.

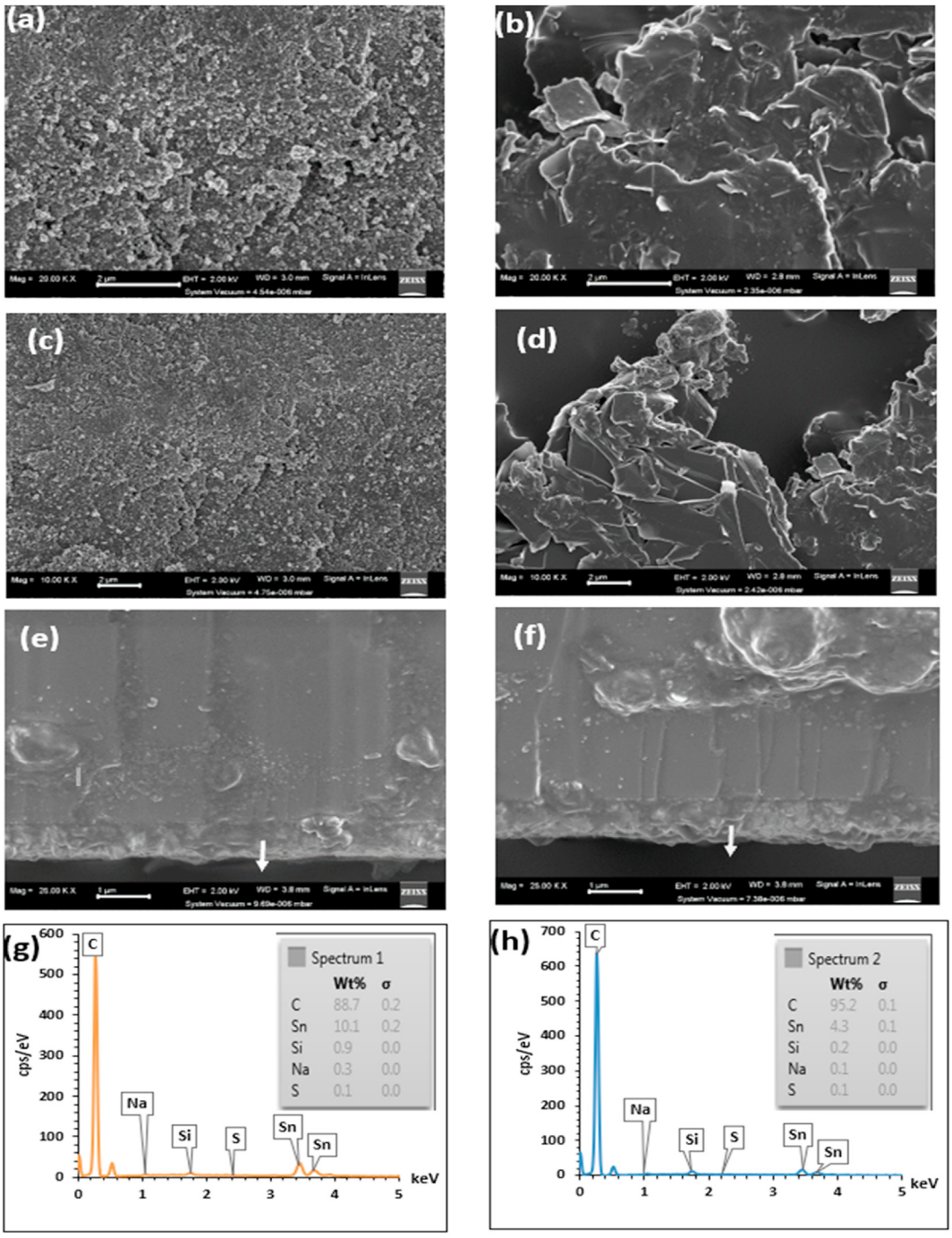

Fig. 6. FE-SEM images, cross-sectional SEM image without the counter electrode and EDS of (a,c,e,g) uncapped SnS and (b,d,f,h) HDA-capped SnS nanoparticles.

Elemental composition analysis of HDA-capped SnS and uncapped SnS was evaluated using EDS, with the corresponding weight percentage constituent elements shown in Fig. 6(g) and (h). From Fig. 6 (g) and (h), the compositional information of the materials are displayed in the form of a calibrated peak-height proportion, with the energy peaks corresponding to the individual elements in the material. The increase in carbon atoms is linked to the temperature effect, similar observation for increase carbon atoms has been reported [49], while the variations in Sn and S is a common occurrence in the thermal process synthesis approach. Elaborate description of this observation have been reported by various studies on many chalcogenide materials [50–53].

3.5. Absorption spectra

To understand the optical behaviour of the as-prepared photosensitizers, LAMBDA 365 UV–Vis spectrophotometer from PerkinElmer was used to obtained the absorption spectra, while PerkinElmer LS 45 fluorimeter was used to obtain the Photoluminescence spectra. Both HDA-capped SnS and uncapped SnS nanoparticles exhibited a predominant absorbance edge in the visible region as shown in Fig. 7 (a, b, c). The emission of visible radiation by both photosensitizers began around 450 nm and reaches a maximum wavelength of around 700 nm, confirming strong absorption in the entire visible region and can be ascribed to the

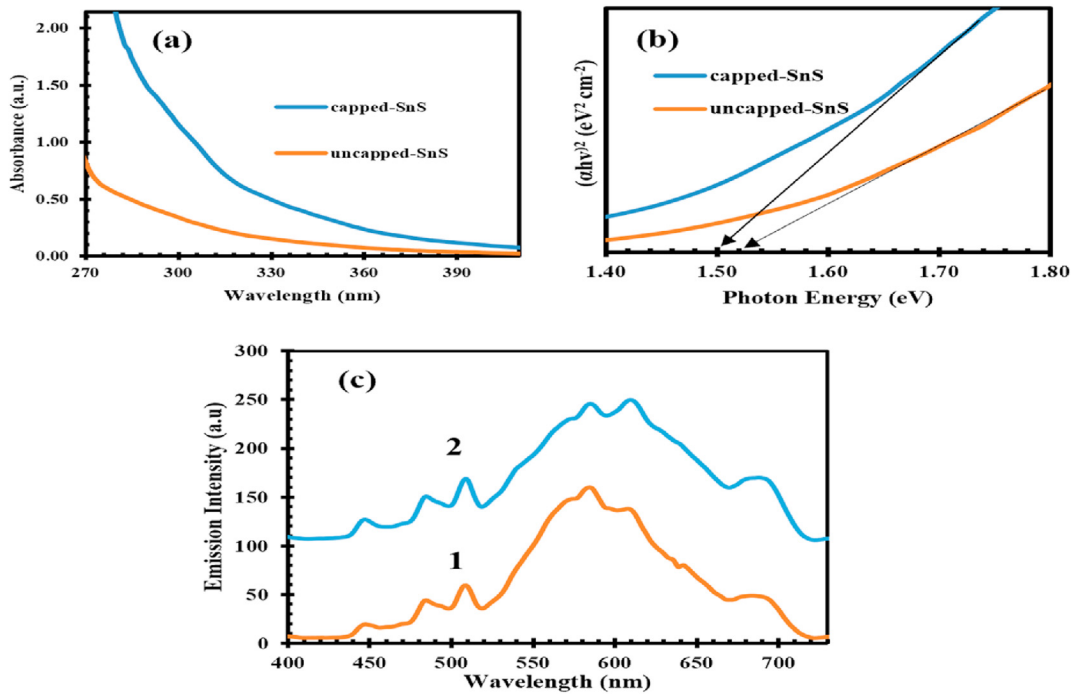

Fig. 7. (a) Absorbance vs wavelength plots uncapped SnS and HDA-capped SnS nanoparticles. (b) Plots of $(\alpha h\nu)^2$ Vs photon energy for the direct bandgap investigation and PL spectra (c) of uncapped SnS (1) and HDA-capped SnS (2) nanoparticles.

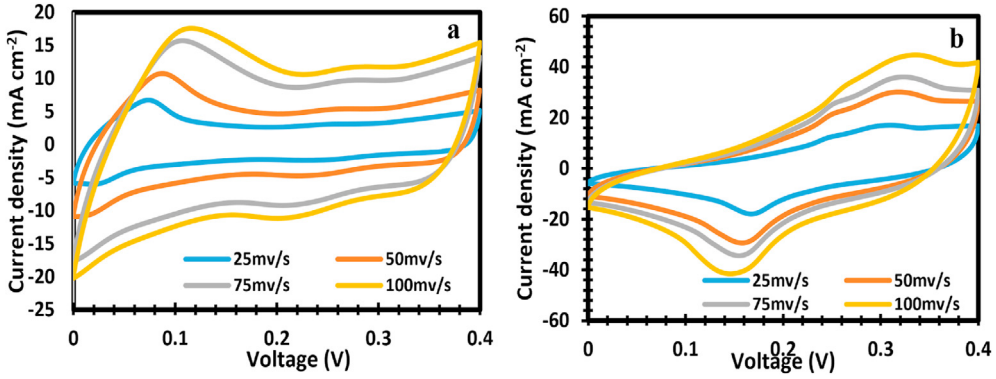

Fig. 8. Cyclic voltammetry curves for (a) uncapped SnS and (b) HDA-capped SnS at difference scan rate.

Table 2
Electrochemical parameters for (a) uncapped SnS and (b) HDA-capped SnS.

Uncapped SnS				
Scan rate	$E_{p,a}$ (V)	$E_{p,c}$ (V)	$\Delta E_p = E_{p,a} - E_{p,c}$ (V)	$E^\circ = ½(E_{p,a} - E_{p,c})$ (V)
25mv/s	0.07	0.02	0.05	0.025
50mv/s	0.09	0.00	0.09	0.045
75mv/s	0.09	0.00	0.09	0.045
100mv/s	0.11	0.00	0.11	0.055
HDA-capped SnS				
25mv/s	0.30	0.17	0.13	0.065
50mv/s	0.32	0.15	0.17	0.085
75mv/s	0.32	0.15	0.17	0.085
100mv/s	0.35	0.15	0.2	0.1

perfect orientation as seen in Fig. 7 (c). These findings are in good agreement with earlier reported values [54–56]. The optical energy direct band gaps were calculated from UV–Vis absorption data using Tauc plot dependence through the following semi empirical expression [57,58]:

$$\alpha h\nu = \beta(h\nu\text{-}E_g)^k \quad (1)$$

where α is the absorption coefficient, h is the plank constant, ν is the frequency of photon, β is a band tailing parameter, E_g is the optical bandgap and k is an exponent factor which depends on the mode of transition and type of the material. Since direct bandgap was determined, $k = 2$ and the intercept of a tangent drawn towards X-axis in the $(\alpha h\nu)^2$ versus (eV) spectra gives the optical energy band gap (Eg) of the nanoparticles. The observed band gaps for HDA-capped SnS and uncapped SnS were found to be 1.50 and 1.52 eV, respectively. These are optimum values needed for the photovoltaic solar energy conversion (1.5 eV). This result is similar to what was reported [59] in recently published work.

3.6. Cyclic voltammetry (CV)

Fig. 8 (a, b) shows typical CV curves of uncapped SnS and HDA-capped SnS photosensitizers while their respective electrochemical parameters at different scan rate from 25 mV/s to 100 mV/s at potential of 0.0–0.4 V is displayed in Table 2. According to Fig. 8 (a), the shifting of

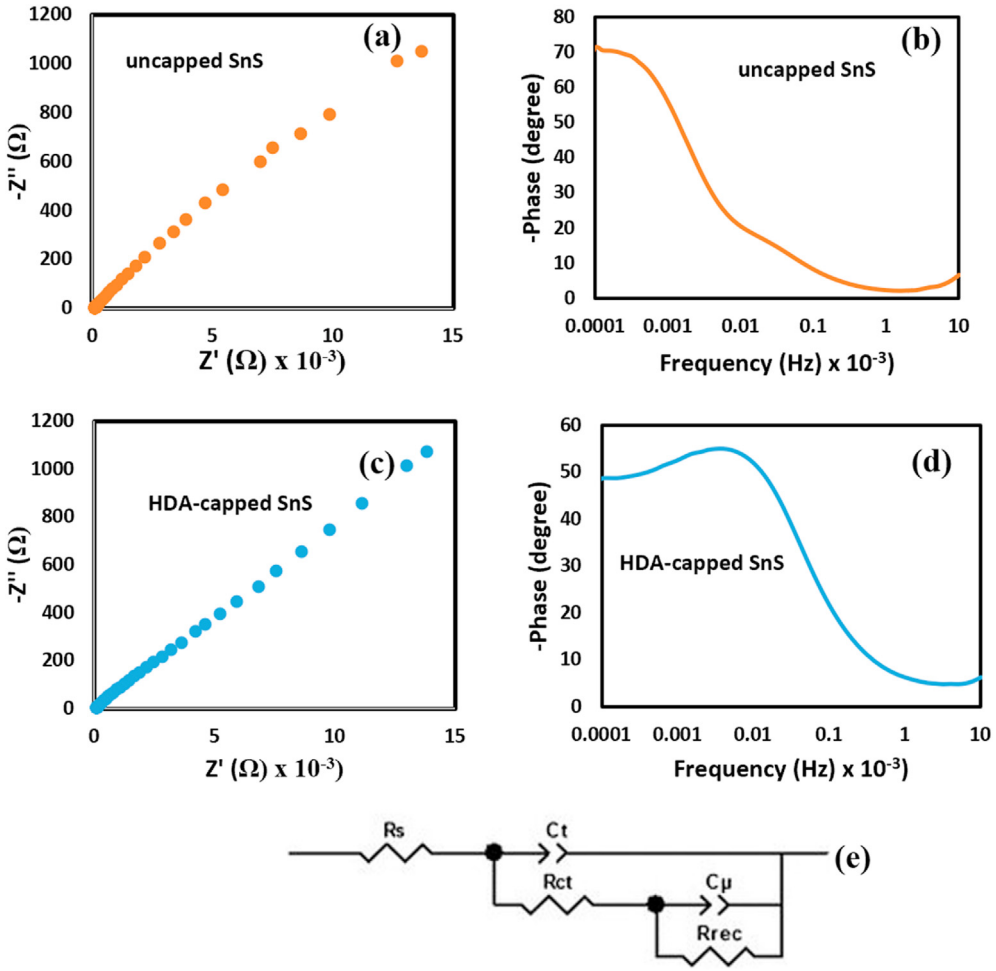

Fig. 9. EIS spectra (a, c) and Bode plots (b, d) of uncapped SnS and HDA-capped SnS and (e) equivalent circuit model for fitting.

the anodic and cathodic peak potentials with an increasing trend, indicates an efficient mass transfer between the electrodes, and the oxidation and reduction of the photosensitizer. All CV curves displays nearly rectangular shapes, which suggests superior capacitive ability rather than faradaic redox capability. The limited redox potential could be detrimental to the quick reduction of the photosensitizer, which is vital in eliminating the possibility of the generated electrons recombining with the oxidised dye molecule. At 100 mV/s the best peak-to-peak separation (ΔE_p) was achieve indicating a good electrical conductivity. At 75 mV/s and 50 mV/s, current peaks were obtained for the uncapped SnS. The uncapped SnS with 25 mV/s performed poorly having the smallest peak. This finding demonstrated that the photosensitizer generated current can produce high current density. Fig. 8 (b), depicts the CV curves and the calculation of corresponding peak-to-peak separation (ΔE_p) for HDA-capped SnS. It could be seen that the high peak separation (ΔE_p) of 0.2 V at 100 mV/s gives rise to slow heterogeneous electron transfer. At 75 mV/s and 50 mV/s 0.17 V were observed, while at 25 mV/s shows a slower peak-to-peak separation than the others due to the structural effects. The 100 mV/s reflected a fast electron transfer with great amount of pore defects [60–63].

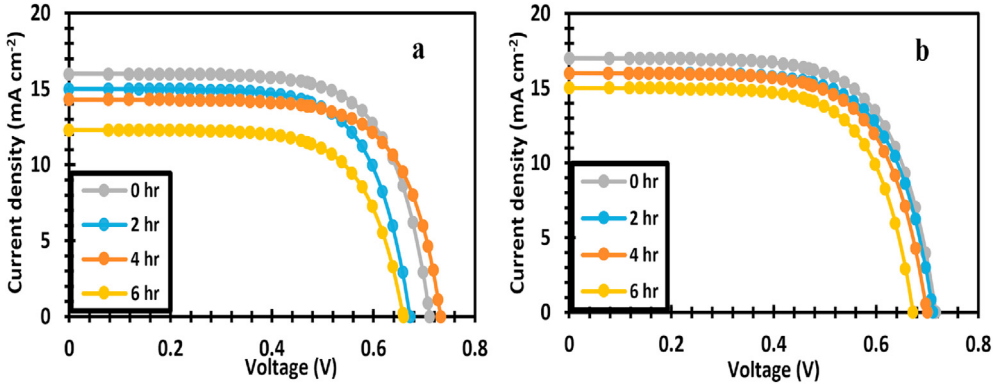

Fig. 10. Current density-voltage for (a) uncapped SnS and (b) HDA-capped SnS.

Table 3
J-V characteristic parameters for (a) uncapped SnS and (b) HDA-capped SnS (mean values ± SD).

Uncapped SnS					
Time	J_{SC} (mA/cm^2)	V_{OC} (V)	*FF*	η (%)	*Pmax (W)*
0 h	16 ± 0.0	0.72 ± 0.4	0.68 ± 0.1	7.83 ± 0.19	7.87
2 h	15 ± 0.3	0.67 ± 0.2	0.68 ± 0.1	6.83 ± 0.01	6.93
4 h	14.30 ± 0.0	0.73 ± 0.1	0.69 ± 0.3	7.20 ± 0.2	7.29
6 h	12.30 ± 0.03	0.65 ± 0.63	0.70 ± 0.4	5.59 ± 0.8	5.53
HDA-capped SnS					
0 h	17 ± 0.0	0.72 ± 0.8	0.67 ± 0.2	8.20 ± 0.4	8.30
2 h	16 ± 0.2	0.72 ± 0.4	0.68 ± 0.8	7.83 ± 0.20	7.85
4 h	16 ± 0.4	0.7 ± 0.6	0.68 ± 0.3	7.61 ± 0.1	7.59
6 h	15 ± 0.02	0.68 ± 0.58	0.68 ± 0.3	6.93 ± 0.7	6.94

3.7. Electrochemical impedance spectroscopy (EIS)

The Nyquist plots for both uncapped and capped SnS sensitizers as seen in Fig. 9 (a) and (c) displayed a higher frequency semicircle. The resistance charge transport (R_1) at the counter electrode/electrolyte interface is due to hemisphere of high frequency. While the charge transport at the TiO_2/photosensitizer/electrolyte interface (R_2) is due to low frequencies. The present work focused mainly on the R_2 to compare the effect of both photosensitizers on the charge transfer and transport at the TiO_2/photosensitizer/electrolyte interface. The interception on the real axis gives equivalent series resistance (ESR) of photosensitizer material, which consists of ionic and electronic contributions. The electronic resistance is connected between the current collector and SnS sensitizer, while the HI-30 electrolyte is related to ionic resistance. The lower ESR values owing to the highly porous nanostructure, which further cemented the SEM results. This promotes smooth access of electrolyte ions to enhance deintercalation and intercalation with low impedance. The diffusion of HDA-capped SnS photosensitizers in HI-30 electrolyte indicates Warburg's constant (*W*) due to the straight line. The HDA-capped SnS sensitizer displayed lower impedance compared to the uncapped SnS sensitizer [26,64–66]. The produced trend shows that the addition of HDA significantly enhanced electron movement between the electrolyte and the photoanode surface.

3.8. Bode plot

The Bode plots displayed in Fig. 9 (b) and (d) show that the frequency peaks shifted from 70 Hz for HDA-capped SnS to 48 Hz for uncapped SnS sensitizer under light illumination. This suggests an improved collection of electrons, lifetime recombination, and faster transport in HDA-capped SnS photosensitizer compared to uncapped SnS [67]. We concluded that the HDA-capped SnS photosensitizer displayed superiority to the uncapped SnS photosensitizer, owing to their ability to reduce electron recombination and enhanced electron lifetime [68].

3.9. Current density-voltage (J–V)

The QDSSCs based on photosensitizers showed very good performance as seen in Fig. 10 (a, b) and Table 3. The high performance of the photosensitizers in the QDSSCs was attributed to the strong absorption of the photosensitizers on the surface of TiO_2, leading to surface passivation and an increase in catalytic reactivity [69,70]. The high catalytic reactivity of the photosensitizers leads to the reaction of the HI-30 electrolyte with electrons generated from the TiO_2, causing recombination as seen in the V_{oc} values. The photosensitizers for both samples at 0hr shows the fill factor (*FF)* of 0.68–0.67 and efficiency (η) of 8.20–7.83% respectively. The P*max* values obtained from both photon absorbers ranges from 5.53 to 7.87 for uncapped SnS and 6.94–8.30 for HDA-capped SnS, this values are comparative to the efficiency of the photosensitizers. The values of *FF* obtained for both photosensitizers implies that recombination has occurred in the solar cell [71–73]. The higher *FF* in the uncapped SnS photosensitizer was due to charge transfer at the interface of the counter electrode/electrolyte and thus, reduced the concentration of the gradients in the electrolyte, recombination rate and the internal resistance as observed in the EIS results. As the time increases to 2hr, the catalytic activity decreases and the conversion efficiency were observed at 6.83% and 7.83% for uncapped SnS and HDA-capped SnS. Further increase in time to 4hr caused the HDA-capped SnS to exhibit an η value of 7.61%, while uncapped SnS efficiency at 7.20% was enhance compare to the 2hr of uncapped SnS. An increase in time to 6hr lead to a decrease in the performance of both samples due to J_{sc} deterioration resulting from poor electrocatalytic activity of the photosensitizers. However, the overall performance was much higher in HDA-capped SnS than the uncapped SnS. The improvement in the HDA-capped SnS as observed in the present study is attributed to the better stability of the aliphatic amines with HDA which gave rise to higher electrocatalytic activity and reduced charge transfer resistance across the interface of the TiO_2/photosensitizer/-electrolyte. Previous studies have shown enhanced conversion efficiency for SnS with additive material as photosensitizer [59,74]. The efficiency obtained from the present study is much higher compared to the studies by Sinsermsuksakul et al. with 4.4% [15] and our previous report with 1.25% [26] which employed the aromatic amine with conjugate, while the present work adopted the aliphatic amine with HDA.

Comparison of incident photon to current conversion efficiency (IPCE) measurement values obtained between 300 and 700 nm for best performing devices suggests an improvement in IPCE value for HDA-capped SnS sensitizer which yielded an IPCE value of 9.1% at 450 nm compared to the uncapped SnS sensitizer with an IPCE value of 6.8% at 450 nm. The enhanced IPCE value obtained for HDA-capped SnS indicates an efficient contribution of absorbed photons to the photocurrent density as a result of improved light absorption and reduced recombination. Further details of the IPCE curves and additional characterization for the sensitizers will be included in subsequent report.4. Conclusions.

In summary, the beneficial properties of *bis*(*N*-diisoproyl-*N*-octyldithiocarbamato) Sn(II) complexes molecular precursor of capped and uncapped SnS were evaluated. HDA capping agent was employed to control the particle size and for surface passivation to enhance electron transfer. HDA idealizes the layer quality by easing the growth of quantum dots SnS, which promotes efficient photon extraction and lower charge recombination. HDA-capped SnS photosensitizer displayed superiority due to good electron lifetime, better shape and size distribution compared to SnS. UV–Vis absorption data using the Tauc plot revealed optimum value at 1.50 eV of energy conversion for HDA-capped SnS. Without HDA capping agent, it was found that uncapped SnS photosensitizer show a poor stability performance compared with HDA-capped SnS after 6 h. It is therefore concluded that the addition of HDA capping agent enhances the performance of HDA-capped SnS compared to SnS photosensitizer. The efficiency of 8.20% obtained from the present study is higher than our previous report [26]. The results from the present study promotes the future prospects of injecting capping agents, as an additional step during fabrication in order to produce optimized high quality QDs photon absorbers for QDSSCs with enhanced reliability, durability and reproducibility performance.

CRediT authorship contribution statement

Mojeed A. Agoro: Conceptualization, Methodology, Validation, Formal analysis, Investigation, Data curation, Writing – original draft, Writing – review & editing, Visualization. **Edson L. Meyer:** Methodology, Resources, Data curation, Validation, Funding acquisition, Visualization, Supervision. **Johannes Z. Mbese:** Methodology, Resources, Data curation, Validation, Funding acquisition, Visualization, Supervision. **Xolile Fuku:** Data curation, Visualization, Validation. **Chinedu C. Ahia:** Methodology, Writing – review & editing, Visualization, Validation, Formal analysis.

Declaration of competing interest

The authors declare that they have no known competing financial interests or personal relationships that could have appeared to influence the work reported in this paper.

Acknowledgement

The authors wish to acknowledge the NRF Thuthuka Grant (GUN: 118139); National Department of Science and Innovation (DST/CON 0170/2019), Eskom TESP (P948); National Research Foundation (GUN: 93215). The authors are also grateful for the financial support by Govan Mbeki Research and Development Centre (GMRDC), University of Fort Hare South Africa.

References

[1] B.A. Hasan, I.H. Shallal, Structural and optical properties of SnS thin films, J. Nano. Adv. Mat. 2 (2014) 43–49.
[2] S.S. Hegde, A.G. Kunjomana, P. Murahari, B.K. Prasad, K. Ramesh, Vacuum annealed tin sulfide (SnS) thin films for solar cell applications, Surface. Interfac. 10 (2018) 78–84.
[3] M.A. Green, Corrigendum to 'Solar cell efficiency tables (version 46), Prog. Photovoltaics Res. Appl. 23 (2015) 805–812. Progress in Photovoltaics: Res. Appl. 2015, 23, 1202-1202.
[4] A. Mukherjee, P. Mitra, Structural and optical characteristics of SnS thin film prepared by SILAR, Mater Sci-Poland 33 (2015) 847–851.
[5] E. Guneri, F. Gode, C. Ulutas, F. Kirmizigul, G. Altindemir, C. Gumus, Properties of p-type SnS thin films prepared by chemical bath deposition, Chalcogenide Lett. 7 (2010) 685–694.
[6] S. Kabouche, Y. Louafi, B. Bellal, M. Trari, Electrochemical growth of SnS thin film: application to the photocatalytic degradation of rhodamine B under visible light, Appl. Phys. A 123 (2017) 545.
[7] V.R.M. Reddy, S. Gedi, C. Park, R. Miles, R.R. Kt, Development of sulphurized SnS thin film solar cells, Curr. Appl. Phys. 15 (2015) 588–598.
[8] J. Kim, J. Kim, S. Yoon, J.Y. Kang, C.W. Jeon, W. Jo, Single phase formation of SnS competing with SnS_2 and Sn_2S_3 for photovoltaic applications: optoelectronic characteristics of thin-film surfaces and interfaces, J. Phys. Chem. 122 (2018) 3523–3532.
[9] X. Hu, G. Song, W. Li, Y. Peng, L. Jiang, Y. Xue, Q. Liu, Z. Chen, J. Hu, Phase-controlled synthesis and photocatalytic properties of SnS, SnS_2 and SnS/SnS_2 heterostructure nanocrystals, Mater. Res. Bull. 48 (2013) 2325–2332.
[10] A.J. Biacchi, D.D. Vaughn, R.E. Schaak, Synthesis and crystallographic analysis of shape-controlled SnS nanocrystal photocatalysts: evidence for a pseudotetragonal structural modification, J. Am. Chem. Soc. 135 (2013) 11634–11644.
[11] E.L. Meyer, J.Z. Mbese, M.A. Agoro, The frontiers of nanomaterials (SnS, PbS and CuS) for dye-sensitized solar cell applications: an exciting new infrared, Material. *Molecules*. 24 (2019) 4223.
[12] S.S. Hegde, A.G. Kunjomana, K.A. Chandrasekharan, K. Ramesh, M. Prashantha, Optical and electrical properties of SnS semiconductor crystals grown by physical vapor deposition technique, Phys. B Condens. Matter 406 (2011) 1143–1148.
[13] J. Zai, K. Wang, Y. Su, X. Qian, J. Chen, High stability and superior rate capability of three-dimensional hierarchical SnS_2 microspheres as anode material in lithium ion batteries, J. Power Sources 196 (2011) 3650–3654.
[14] I.Y. Ahmet, M. Guc, Y. Sánchez, M. Neuschitzer, V. Izquierdo-Roca, E. Saucedo, A.L. Johnson, Evaluation of AA-CVD deposited phase pure polymorphs of SnS for thin films solar cells, RSC Adv. 9 (2019) 14899–14909.
[15] P. Sinsermsuksakul, L. Sun, S.W. Lee, H.H. Park, S.B. Kim, C. Yang, R.G. Gordon, Overcoming efficiency limitations of SnS-based solar cells, Adv. Energy Mater. 4 (2014) 1400496.
[16] B. Ghosh, M. Das, P. Banerjee, S. Das, Fabrication of vacuum-evaporated SnS/CdS heterojunction for PV applications, Sol. Energy Mater. Sol. Cells 92 (2008) 1099–1104.
[17] T. Minemura, K. Miyauchi, K. Noguchi, K. Ohtsuka, H. Nakanishi, M. Sugiyama, Preparation of SnS films by low temperature sulfurization, Phys. Status Solidi C 6 (2009) 1221–1224.
[18] K.T.R. Reddy, N.K. Reddy, R.W. Miles, Photovoltaic properties of SnS based solar cells, Sol. Energy Mater. Sol. Cells 90 (2006) 3041–3046.
[19] S. Banu, S.J. Ahn, Y.J. Eo, J. Gwak, A. Cho, Tin monosulfide (SnS) thin films grown by liquid-phase deposition, Sol. Energy 145 (2017) 33–41.
[20] S. Omeiri, B. Hadjarab, M. Trari, Photoelectrochemical properties of anodic silver sulphide thin films, Thin Solid Films 519 (2011) 4277–4281.
[21] O.E. Ogah, G. Zoppi, I. Forbes, R.W. Miles, Thin films of tin sulphide for use in thin film solar cell devices, Thin Solid Films 517 (2009) 2485–2488.
[22] A. Akkari, C. Guasch, N. Kamoun-Turki, Chemically deposited tin sulphide, J. Alloys Compd. 490 (2010) 180–183.
[23] K.S. Kumar, C. Manoharan, S. Dhanapandian, A.G. Manohari, T. Mahalingam, Effect of indium incorporation on properties of SnS thin films prepared by spray pyrolysis, Optik 125 (2014) 3996–4000.
[24] N. Pradhan, B. Katz, S. Efrima, Synthesis of high-quality metal sulfide nanoparticles from alkyl xanthate single precursors in alkylamine solvents, J. Phys. Chem. B 107 (2003) 13843–13854.
[25] A.E. Oluwalana, P.A. Ajibade, Effect of temperature and capping agents on structural and optical properties of tin sulphide nanocrystals, J. Nanotechnol. (2019).
[26] J.Z. Mbese, E.L. Meyer, M.A. Agoro, Electrochemical performance of photovoltaic cells using HDA capped-SnS nanocrystal from *bis(N*-1,4-Phenyl-*N*-Morpho-Dithiocarbamato) Sn(II) complexes, Nanomaterials 10 (2020) 414.
[27] E.L. Meyer, J.Z. Mbese, M.A. Agoro, R. Taziwa, Optical and structural-chemistry of SnS nanocrystals prepared by thermal decomposition of *bis(N*-diisopropyl-*N*-octyl dithiocarbamato) tin(II) complex for promising materials in solar cell applications, Opt. Quant. Electron. 52 (2020) 90.
[28] M.A. Agoro, E.L. Meyer, J.Z. Mbese, K. Manu, Electrochemical fingerprint of CuS-Hexagonal chemistry from (*bis(N*-1,4-Phenyl-*N*-(4-Morpholinedithiocarbamato) copper(II) complexes) as photon absorber in quantum-dot/dye-sensitised solar cells, Catalysts 10 (2020) 300.
[29] M.A. Agoro, J.Z. Mbese, E.L. Meyer, K. Onyenankeya, Electrochemical signature of CuS photosensitizers thermalized from alkyldithiocarbamato Cu(II) molecular precursors for quantum dots sensitized solar cells, Mater. Lett. 285 (2021), 129191.
[30] M.A. Agoro, J.Z. Mbese, E.L. Meyer, Electrochemistry of inorganic OCT-PbS/HDA and OCT-PbS photosensitizers thermalized from *bis(N*-diisopropyl-*N*-octyldithiocarbamato) Pb(II) molecular precursors, Molecules 25 (2020) 1919.
[31] H. Kafashan, M. Azizieh, Z. Balak, Electrochemical synthesis of nanostructured Se-doped SnS: effect of Se-dopant on surface characterizations, Appl. Surf. 410 (2017) 186–195.
[32] F. Jamali-Sheini, M. Cheraghizade, R. Yousefi, SnS nanosheet films deposited via thermal evaporation: the effects of buffer layers on photovoltaic performance, Sol. Energy Mater. Sol. Cells 154 (2016) 49–56.
[33] C. Lin, M. Zhu, T. Zhang, Y. Liu, Y. Lv, X. Li, M. Liu, Cellulose/SnS_2 composite with enhanced visible-light photocatalytic activity prepared by microwave-assisted ionic liquid method, RSC Adv. 7 (2017) 12255–12264.
[34] K.S. Kumar, A.G. Manohari, S. Dhanapandian, T. Mahalingam, Physical properties of spray pyrolyzed Ag-doped SnS thin films for opto-electronic applications, Mater. Lett. 131 (2014) 167–170.
[35] S. Sebastian, I. Kulandaisamy, S. Valanarasu, I.S. Yahia, H.S. Kim, D. Vikraman, Microstructural and electrical properties evaluation of lead doped tin sulfide thin films, J. Sol. Gel Sci. Technol. 93 (2020) 52–61.
[36] L.T. Yarce, E.R. Andres, R.R. Trujillo, C.M. Ruiz, T.D. Becerril, R.S. Gonzalez, R.G. Isasmendi, A.C. Solis, G.G. Salgado, The morphological changes of SnS thin films deposited on stainless-steel substrates at low temperatures, EJET 4 (2019) 1–4.
[37] A. Bhorde, A. Pawbake, P. Sharma, S. Nair, A. Funde, P. Bankar, M. More, S. Jadkar, Solvothermal synthesis of tin sulfide (SnS) nanorods and investigation of its field emission properties, Appl. Phys. A 124 (2018) 1–8.
[38] A.S. Sarkar, A. Mushtaq, D. Kushavah, S.K. Pal, Liquid exfoliation of electronic grade ultrathin tin (II) sulfide (SnS) with intriguing optical response, NPJ 2D Mater. Appl. 4 (2020) 1–9.
[39] September B.H. Baby, D.B. Mohan, Phase formation study of SnS nanoparticles synthesized through PVP assisted polyol method, IOP Conf. Ser. Mater. Sci. Eng. 360 (2018), 012003.
[40] S. Sebastian, I. Kulandaisamy, A.M.S. Arulanantham, S. Valanarasu, A. Kathalingam, A.J. Jebathew, M. Shkir, M. Karunakaran, Influence of Al doping concentration on the opto-electronic chattels of SnS thin films readied by NSP, Opt. Quant. Electron. 51 (2019) 100.
[41] R. Kihal, H. Rahal, A.M. Affoune, M. Ghers, Electrodeposition of SnS thin film solar cells in the presence of sodium citrate, J. Electrochem. Sci. Technol. 8 (3) (2017) 206–214.
[42] M. Al-Shakban, Z. Xie, N. Savjani, M.A. Malik, P. O'Brien, A facile method for the production of SnS thin films from melt reactions, J. Mater. Sci. 51 (13) (2016) 6166–6172.
[43] Y. Oda, H. Shen, L. Zhao, J. Li, M. Iwamoto, H. Lin, Energetic alignment in nontoxic SnS quantum dot-sensitized solar cell employing spiro-OMeTAD as the solid-state electrolyte, Sci. Technol. Adv. Mater. 15 (2014), 035006.
[44] S. Jayswal, R.S. Moirangthem, Construction of a solar spectrum active SnS/ZnO p–n heterojunction as a highly efficient photocatalyst: the effect of the sensitization process on its performance, New J. Chem. 42 (2018) 13689–13701.
[45] P. Kevin, D.J. Lewis, J. Raftery, M.A. Malik, P. O'Brien, Thin films of tin(II) sulphide (SnS) by aerosol-assisted chemical vapour deposition (AACVD) using tin(II) dithiocarbamates as single-source precursors, J. Cryst. Growth 415 (2015) 93–99.
[46] J. Akhtar, M.A. Malik, P. O'Brien, M. Helliwell, Controlled synthesis of PbS nanoparticles and the deposition of thin films by Aerosol-Assisted Chemical Vapour Deposition (AACVD), J. Mater. Chem. 20 (2010) 6116–6124.
[47] S.S. Hortikar, V.S. Kadam, A.B. Rathi, C.V. Jagtap, H.M. Pathan, I.S. Mulla, P.V. Adhyapak, Synthesis and deposition of nanostructured SnS for semiconductor-sensitized solar cell, J. Solid State Electrochem. 21 (2017) 2707–2712.
[48] Z. Zolfaghari-Isavandi, Z. Shariatinia, Fabrication of CdS quantum dot sensitized solar cells using nitrogen functionalized CNTs/TiO_2 nanocomposites, Diam. Relat. Mater. 81 (2018) 1–15.
[49] D.C. Onwudiwe, P.A. Ajibade, Thermal studies of Zn(II), Cd(II) and Hg(II) complexes of some N-alkyl-N-phenyl-dithiocarbamates, Int. J. Mol. Sci. 13 (2012) 9502–9513.
[50] Z.Y. Zhong, E.S. Cho, S.J. Kwon, Effect of substrate temperatures on evaporated In_2S_3 thin film buffer layers for Cu (In, Ga) Se_2 solar cells, Thin Solid Films 547 (2013) 22–27.

[51] K. Saritha, S. Rasool, K.R. Reddy, A.M. Saad, M.S. Tivanov, S.E. Tikoto, O.V. Korolik, V.F. Gremenok, Substrate temperature dependent physical properties of SnS_{1-x} Se_x thin films, Appl. Phys. A 125 (2019) 704.
[52] L. Wang, H. Zhai, G. Jin, X. Li, C. Dong, H. Zhang, B. Yang, H. Xie, H. Sun, 3D porous ZnO–SnS p–n heterojunction for visible light driven photocatalysis, Phys. Chem. Chem. Phys. 19 (2017) 16576–16585.
[53] I. Shown, S. Samireddi, Y.C. Chang, R. Putikam, P.H. Chang, A. Sabbah, F.Y. Fu, W.F. Chen, C.I. Wu, T.Y. Yu, P.W. Chung, Carbon-doped SnS_2 nanostructure as a high-efficiency solar fuel catalyst under visible light, Nat. Commun. 9 (2018) 1–10.
[54] S. Baskoutas, A.F. Terzis, Size-dependent band gap of colloidal quantum dots, J. Appl. Phys. 99 (2006), 013708.
[55] S. Sohila, M. Rajalakshmi, C. Muthamizhchelvan, S. Kalavathi, C. Ghosh, R. Divakar, C.N. Venkiteswaran, N.G. Muralidharan, A.K. Arora, E. Mohandas, Synthesis and characterization of SnS nanosheets through simple chemical route, Mater. Lett. 65 (2011) 1148–1150.
[56] J. Henry, K. Mohanraj, S. Kannan, S. Barathan, G. Sivakumar, Structural and optical properties of SnS nanoparticles and electron-beam-evaporated SnS thin films, J. Exp. Nanosci. 10 (2015) 78–85.
[57] P. Mani, K. Manikandan, Infleunce of molar concentration on ethylene diamine tetra acetic acid (EDTA) added to tin sulfide (SnS) thin films grown by silar method, J. Mater. Sci.: Mater. Electron. 28 (2017) 13602–13612.
[58] V.K. Arepalli, T. Dai Nguyen, J. Kim, Influence of Ag thickness on the structural, optical, and electrical properties of the SnS/Ag/SnS trilayer films for solar cell application, Curr. Appl. Phys. 20 (2020) 438–444.
[59] D. Sharma, N. Kamboj, K. Agarwal, B.R. Mehta, Structural, optical and photoelectrochemical properties of phase pure SnS and SnS_2 thin films prepared by vacuum evaporation method, J. Alloys Compd. 822 (2020) 153653.
[60] X. Chen, Y. Hou, B. Zhang, X.H. Yang, H.G. Yang, Low-cost SnS_x counter electrodes for dye-sensitized solar cells, Chem. Commun. 49 (2013) 5793–5795.
[61] F. Alam, V. Dutta, Tin sulfide (SnS) nanostructured films deposited by continuous spray pyrolysis (CoSP) technique for dye-sensitized solar cells applications, Appl. Surf. Sci. 358 (2015) 491–497.
[62] M.S. Mahmoud, M. Motlak, N.A. Barakat, Facile synthesis and characterization of two dimensional SnO_2-decorated graphene Oxide as an effective counter electrode in the DSSC, Catalysts 9 (2019) 139.
[63] R. Gao, Z. Liang, J. Tian, Q. Zhang, L. Wang, G. Cao, ZnO nanocrystallite aggregates synthesized through interface precipitation for dye-sensitized solar cells, Nano Energy 2 (2013) 40–48.
[64] M.D. Tyona, S.B. Jambure, C.D. Lokhande, A.G. Banpurkar, R.U. Osuji, F.I. Ezema, Dye-sensitized solar cells based on Al-doped ZnO photoelectrodes sensitized with rhodamine, Mater. Lett. 220 (2018) 281–284.
[65] E.O. Onah, S.U. Offiah, U.K. Chime, G.M. Whyte, R.M. Obodo, O.V. Ekechukwu, I. Ahmad, P.E. Ugwuoke, F.I. Ezema, Comparative photo-response performances of dye sensitized solar cells using dyes from selected plants, Surface. Interfac. 20 (2020) 100619.
[66] A. Patil, A. Lokhande, P. Shinde, H. Shelke, C. Lokhande, Electrochemical supercapacitor properties of SnS thin films deposited by low-cost chemical bath deposition route, Int. J. Eng. 10 (2017) 914–922.
[67] K.S. Kumar, A.G. Manohari, S. Dhanapandian, T. Mahalingam, Physical properties of spray pyrolyzed Ag-doped SnS thin films for opto-electronic applications, Mater. Lett. 131 (2014) 167–170.
[68] J. Chao, Z. Wang, X. Xu, Q. Xiang, W. Song, G. Chen, J. Hu, D. Chen, Tin sulfide nanoribbons as high performance photoelectrochemical cells, flexible photodetectors and visible-light-driven photocatalysts, RSC Adv. 3 (2013) 2746–2753.
[69] C. Yuan, L. Li, J. Huang, Z. Ning, L. Sun, H. Ågren, Improving the photocurrent in quantum-dot-sensitized solar cells by employing alloy PbxCd1 − xS quantum dots as photosensitizers, Nanomaterials 6 (2016) 97.
[70] M. Cheraghizade, F. Jamali-Sheini, R. Yousefi, F. Niknia, M.R. Mahmoudian, M. Sookhakian, The effect of tin sulfide quantum dots size on photocatalytic and photovoltaic performance, Mater. Chem. Phys. 195 (2017) 187–194.
[71] F. Fabregat-Santiago, G. Garcia-Belmonte, I. Mora-Sero, J. Bisquert, Characterization of nanostructured hybrid and organic solar cells by impedance spectroscopy, Phys. Chem. Chem. Phys. 13 (2011) 9083–9118.
[72] M. Devika, N. Koteeswara Reddy, M. Prashantha, K. Ramesh, S. Venkatramana Reddy, Y.B. Hahn, K.R. Gunasekhar, The physical properties of SnS films grown on lattice-matched and amorphous substrates, Phys. Status Solidi 207 (2010) 1864–1869.
[73] M. Patel, A. Ray, Magnetron sputtered Cu doped SnS thin films for improved photoelectrochemical and heterojunction solar cells, RSC Adv. 4 (2014) 39343–39350.
[74] H. Kafashan, Comparison the effects of Se and Te inclusion on the physical and electrochemical properties of SnS thin films, Mater. Sci. Semicond. Process. 88 (2018) 148–160.